Piezo-dependent surveillance of matrix stiffness generates transient cells that repair the basement membrane

Aubrie M. Stricker[1], M. Shane Hutson[2], Andrea Page-McCaw[1,3]

[1]Department of Cell and Developmental Biology, Center for Matrix Biology, Program in Developmental Biology, Vanderbilt University, Nashville, TN, USA

[2]Department of Physics and Astronomy, Department of Biological Sciences, Vanderbilt University, Nashville, TN, USA

[3]Lead contact: andrea.page-mccaw@vanderbilt.edu

Summary

Basement membranes are extracellular matrix sheets separating tissue layers and providing mechanical support, and Collagen IV (Col4) is their most abundant protein. Although basement membranes are repaired after damage, little is known about repair, including whether and how damage is detected, what cells repair the damage, and how repair is controlled to avoid fibrosis. Using the intestinal basement membrane of adult *Drosophila* as a model, we show that after basement membrane damage, there is a sharp increase in enteroblasts transiently expressing Col4, or “matrix mender” cells. Enteroblast-derived Col4 is specifically required for matrix repair. The increase in matrix mender cells requires the mechanosensitive ion channel Piezo, expressed in intestinal stem cells. Matrix menders are induced by the loss of matrix stiffness, as specifically inhibiting Col4 crosslinking is sufficient for Piezo-dependent induction of matrix mender cells. Our data suggest that epithelial stem cells control basement membrane integrity by monitoring stiffness.

Keywords: Basement membrane, *Drosophila*, Collagen IV, midgut, Piezo, matrix, tensional stiffness, intestinal stem cells, enteroblasts, repair

Introduction

Extracellular matrix (ECM) is an essential conserved component of all animal tissues. In addition to providing structural support, ECM influences cell adhesion, shape, signaling, and behaviors. When tissues are damaged, ECM needs to be repaired, and pathological ECM damage is a feature of many human diseases[1,2]. Despite the critical importance of ECM repair, little is known about the cellular processes and molecular signals that orchestrate repair. At the most fundamental level, it is unknown whether and how cells detect ECM damage. Moreover, ECM proteins, including collagens, are among the most stable proteins in the body, with the longest-lived exhibiting half-lives on the order of an animal's lifetime[3–6]. ECM longevity presents a challenge, as repairing with excess ECM causes fibrosis. In this study, we identify a mechanism that cells use to sense damaged matrix, and they respond by transiently producing matrix until repair is completed.

ECM can be subdivided into two types, stromal matrix and basement membrane, the focus of this study. Basement membranes are thin sheets that underlie epithelia and wrap around muscles and organs. Their most abundant protein is Collagen IV (Col4), a heterotrimer that self-assembles *in vitro* into networks and provides structural support[7]. Self-assembly raises questions about the nature of basement membrane repair. Is there a continuing self-assembly process for maintenance that also functions passively to repair damage? Or is repair an active process, with cells sensing damage and directing repair?

Basement membranes are ancient, arising along with multicellularity itself[8]. Given the evolutionary conservation, *Drosophila* offers an excellent model to address

60 questions of basement membrane homeostasis and repair. Flies have the same
61 basement membrane structure and composition as mammals, with all the main
62 components but fewer copies. There is only one type IV collagen (Col4) heterotrimer
63 composed of the two collagen subunits Col4a1 and Col4a2 (aka Viking, Vkg); there are
64 two laminin heterotrimers, one nidogen gene, and one perlecan gene[9]. Functional GFP-
65 tagged alleles of Vkg offer tremendously powerful reagents for imaging and genetics[10].
66 We use the *Drosophila* posterior midgut as a model to analyze basement membrane
67 repair. The fly gut is a monolayer epithelium derived from stem cells that generate two
68 lineages, enterocytes and enteroendocrine cells, with intermediates in between[11–13].
69 Between the epithelium and the surrounding peristalsis muscles there is basement
70 membrane, and it is continuous with the basement membrane enveloping the muscles
71 (Fig. 1A). We damage the basement membrane by feeding the flies dextran sodium
72 sulfate (DSS), which gets visibly lodged in the gut basement membrane, fractures its
73 structure, and reduces its stiffness[14]. After stopping DSS feeding, basement membrane
74 repair occurs within two days, providing a temporal window for analyzing repair[14].
75 In this study, we find that genes encoding all major basement membrane
76 components are required for both repair and maintenance. However, after damage, the
77 source of Col4 for the midgut changes: without damage, Col4 originates from the fat
78 body, but after damage, Col4 is transiently expressed locally by gut epithelial cells we
79 call “matrix menders,” which are specialized short-lived enteroblasts. Knocking down
80 Col4 in enteroblasts specifically inhibits gut basement membrane repair. For damage to
81 induce matrix menders requires the mechanosensitive channel *Piezo*, expressed in
82 neighboring intestinal stem cells (ISCs). Indeed, specifically reducing basement

83 membrane stiffness by reducing Col4 crosslinking is sufficient to induce matrix-mender
84 cells in a Piezo-dependent manner. Our results suggest that epithelial stem cells surveil
85 basement membrane integrity by monitoring its stiffness, responding to defects by
86 generating short-lived repair cells.
87

88 **Results**

89 **Basement membrane repair and maintenance require many of the same**
90 **components.**

91 DSS directly damages the posterior midgut basement membrane of *Drosophila*[14].
92 After ingestion, DSS is transported through enterocytes to accumulate in the adjacent
93 basement membrane (Fig. 1A). This mechanism is different from mice, where DSS is
94 excluded by the intact epithelium[14,15]. In flies, DSS damages basement membranes,
95 making them visibly fractured as visualized by TEM, less dense as measured with
96 fluorescence and super-resolution microscopy, and less stiff as measured in a tensile
97 strain assay[14]. The basement membrane mechanical damage changes the shape of the
98 gut peristalsis muscles, which are outlined by Col4 (Fig. 1A, right side). A similar muscle
99 shape is observed in fly guts lacking the Col4 crosslinking enzyme Peroxidasin
100 (Pxn)[14,16,17], and these basement membranes also have reduced tensile stiffness[14,17,18].
101 In both instances, gut muscles become dysmorphic when enveloped by weakened
102 basement membrane, and thus we can infer basement membrane stiffness from gut
103 muscle shape, measured as aspect ratio. Importantly, two days after removing DSS and
104 feeding flies regular food, there is full restoration of basement membrane structure and
105 the muscle shape[14].

106 Previously, we determined that repair after DSS damage requires synthesis of
107 new basement membrane proteins, including *vkg*, *LamininB1*, and *Pxn*[14]. We asked
108 whether other conserved basement membrane components were required for repair,
109 targeting Perlecan (*trol*), Nidogen (*Ndg*), and the Col4 extracellular chaperone, *SPARC*.
110 We used two different RNAi lines to knock them down everywhere with *TubP-Gal4*,

111 initiating knockdown in 6-day old adult females. After two days, flies were fed DSS for
112 two days, then repair was allowed for two days (6 days total knockdown). By analyzing
113 muscle shape (aspect ratio), we found *trol*, *Ndg*, and *SPARC* were all required for
114 basement membrane repair (Fig. S1A-F). The requirement for new basement
115 membrane proteins indicates that damaged basement membranes are replaced with
116 new matrix. These same proteins are required for basement membrane maintenance
117 without externally applied damage, as knocking down *trol*, *Ndg,* or *SPARC* for 10 days
118 in adults caused dysmorphic gut muscles (Fig. S1K-P), whereas knocking down non-
119 matrix extracellular proteins *Gbp1* or *Gbp2*[19] had no effect (Fig. S1G-J, Q-T). From this,
120 we conclude that although basement membrane is replaced during normal homeostatic
121 maintenance, it is replaced faster during repair.
122

123 **Collagen IV is upregulated in matrix mender cells following damage.**

124 Although basement membranes are maintained throughout the body, we expect
125 damage-triggered repair to be a localized process. The Col4 in many *Drosophila* tissues
126 originates from a distant organ, the fat body[20,21], and we found that was true for the
127 undamaged gut by expressing tissue-specific dsRNA against GFP in *vkg-GFP/vkg+*
128 heterozygotes. *vkg-GFP/vkg+* gut basement membranes fluoresce green, but when
129 dsRNA against GFP was expressed ubiquitously with *TubP-Gal4*, there was virtually no
130 gut fluorescence, demonstrating the effectiveness of heterozygous knockdown (Fig S2
131 A-D). Importantly, the knockdown animal is functionally equivalent to a *vkg*
132 heterozygote, viable and healthy[21], so we do not expect to trigger any compensatory
133 mechanisms. When GFP was knocked down specifically in the fat body with *c564-Gal4*,

134 gut fluorescence was also extremely low, similar to ubiquitous knockdown (Fig. 1B,C
135 and Fig. S2A-D; specificity of *c564-Gal4* shown in Fig. S2I,J), indicating most of the
136 midgut Col4 originates from the fat body, a distant source. However, when these
137 animals were fed DSS to damage the gut basement membrane, the gut fluorescence
138 level increased significantly, indicating that Col4 was coming from another source
139 besides the fat body during repair (Fig. 1C-E; see also Fig. SE-H). In cross-section, the
140 DSS-induced Vkg-GFP was deposited between the gut epithelium and peristalsis
141 muscles, suggesting a local source of Col4 specific for repair (Fig. 1F,G).

142 To identify a damage-specific local source of Col4, we used *Cg-Gal4*, a reporter
143 of Collagen IV gene expression in which Gal4 is under control of a collagen enhancer
144 that lies between the head-to-head promoters of the two collagen genes *Col4a1* and
145 *vkg*[22]. In control guts, only a few cells in the posterior midgut (R4) faintly expressed
146 *Cg>GFP,* but after 2 d of DSS damage the number and intensity of *Cg>GFP* cells in the
147 gut increased substantially, from 1.8% to 5.7% of gut epithelial cells (Fig. 1H-M, Fig.
148 S3A). Analyzing their numbers over time, we found that *Cg>GFP* cells increased after
149 only one day of DSS feeding, peaked after the second day of DSS, and then subsided
150 after DSS is removed. Interestingly, *Cg>GFP* expression was no longer observed 2
151 days after DSS removal, when the gut basement membrane was repaired (Fig. 1L). We
152 dubbed these *Cg>GFP* cells “matrix menders” because they express Col4 in response
153 to basement membrane damage but not after repair is complete. Analyzing other genes
154 required for basement membrane repair, we found that reporters for *Pxn* and *Laminin*
155 expression (*Pxn>GFP* and *LanB1>GFP*) were active in the gut without basement

156 membrane damage; the number of *Pxn*-expressing cells doubled after damage, but the
157 number of *LanB1*-expressing cells did not increase (Fig. S4).
158
159 **Matrix menders arise in response to basement membrane damage rather than**
160 **epithelial damage.**
161 In addition to damaging basement membranes, DSS also damages cells[23]. To
162 assess the damage profile that induces matrix menders, we tested two additional drugs
163 known to damage the fly gut. Bleomycin is a DNA-damaging agent that targets
164 enterocytes, causing tissue disorganization, cell loss, and a resulting increase in stem
165 cell divisions[23]. After feeding bleomycin for 2 days, DNA damage was evident by anti-
166 H2AvD staining and increased stem cell divisions were evident by anti-pH3 staining
167 (Fig. S3B,C), yet the basement membranes remained undamaged as determined by
168 muscle shape, and matrix mender cells were not evident (Fig. 1N-Q). Next we tested
169 paraquat, which damages the fly gut by inducing reactive oxygen species and
170 increasing stem cell divisions[24,25]. Feeding flies paraquat for 16 h, reported to maximize
171 damage without causing lethality[24], caused unexpected basement membrane damage,
172 evident by altered muscle shape, and it significantly induced matrix menders (Fig. 1R-
173 U), similar to the levels seen in response to DSS. These results indicate that matrix
174 mender cells arise specifically to basement membrane damage, rather than epithelial
175 damage.
176
177 **Matrix menders are a subset of enteroblasts.**

178 The cell types of the fly posterior midgut are well known (Fig. 2A) and can be
179 identified with established cell markers. In DSS-fed guts, the Cg>GFP matrix menders
180 did not express the intestinal stem cell marker Dl, but interestingly, about 75% of matrix
181 menders were adjacent to Dl+ stem cells (174/236), suggesting that matrix menders are
182 either enteroblasts or pre-enteroendocrine cells. Nearly all *Cg>GFP* labeled matrix
183 menders were positive for the enteroblast marker *Su(H)GBE-lacZ*, indicating that matrix
184 menders are enteroblasts (Fig. 2B,C). Not all enteroblasts are matrix menders,
185 however, as only 43% of the *Su(H)GBE*-positive enteroblasts were also positive for
186 *Cg>GFP* (Fig. 2C). In guts that were not damaged by DSS, *Cg*-expressing cells were
187 still enteroblasts (81%) but fewer enteroblasts expressed *Cg* (21%) (Fig. 2C). Thus,
188 some but not all enteroblasts are matrix menders. The number of enteroblasts is known
189 to increase in response to DSS[23], and we found that after 2 d of DSS, the number of
190 enteroblasts increased from an average of ~7/100 cells to ~11/100 cells (Fig. 2D and
191 Fig. S6A). Nearly all this increase in enteroblasts can be accounted for by the increase
192 in collagen-expressing matrix mender cells (Fig. 1L).
193

194 **Collagen IV from enteroblasts is required for repair.**

195 We wanted to determine if the Col4 from matrix-mender enteroblasts was
196 important for repair, but unfortunately knocking down Col4 with *Cg-Gal4* would target
197 collagen in other tissues, such as the fat body. Instead, we knocked down *Col4a1* in
198 specific cell types with different Gal4 drivers, including the enteroblast driver *Su(H)GBE-*
199 *Gal4* (Fig. 2E). With collagen removed from each potential source, we compared gut
200 morphology in undamaged guts to those that were DSS-damaged and allowed to repair,

201 scoring samples blinded to identity or treatment. When *Col4a1* was knocked down in
202 the fat body with *c564-Gal4*, many guts had dysmorphic muscles even without damage,
203 and morphology was similar when treated with DSS and allowed to repair; these results
204 indicate that Col4 from the fat body is important for gut basement membrane
205 development or homeostasis as expected, but it is not specific for repair. We next
206 knocked down Col4a1 in enteroblasts with *Su(H)GBE-Gal4,* which includes matrix
207 menders; although *Su(H)GBE* is expressed in some larval tissues including wing and
208 tracheae[26], it is not expressed in known collagen source tissues (adult fat body,
209 Malpighian tubules, or ovary, Fig. S5D-G). Gut muscle morphology was normal without
210 DSS treatment, but repair was severely compromised, with 70% still damaged two days
211 after removing DSS. To confirm the specificity of RNAi-mediated knockdown, we
212 knocked down *vkg* (Col4a2) with *Su(H)GBE-Gal4*, and this also interfered specifically
213 with repair and not development (Fig. S5A,B). These results indicate that Col4 from the
214 matrix mender cells is required specifically for midgut basement membrane repair.
215 When *Col4a1* was knocked down with *Myo1a-Gal4* in enterocytes, the terminally
216 differentiated cell type arising from enteroblasts, guts appeared like no-knockdown
217 controls, normal both without damage and after repair; these results indicate that after
218 differentiation, enterocytes do not supply Col4 for development, homeostasis, or repair.
219 We also knocked down *Col4a1* in the intestinal stem cells and enteroendocrine cells
220 (Fig. S5C), and morphology appeared similar without damage and after repair. Only the
221 collagen from enteroblasts is specific for gut basement membrane repair.
222

223 **Most matrix menders are removed from the gut epithelium after repair.**

224 We were interested in what happened to the matrix mender cells after repair,
225 when they were no longer evident. Did they turn off collagen expression, did they
226 differentiate, or did they die? To address this question, we performed lineage tracing of
227 the *Cg-Gal4* expressing matrix menders using the G-TRACE system[27], in which cells
228 actively expressing Col4 were labeled with *nlsRFP* and cells that previously expressed
229 Col4 were permanently labeled with nlsGFP (Fig. 2F). We analyzed the number and
230 fate of collagen-expressing cells in the gut, and as expected, the RFP+ cells behaved
231 like the *Cg>GFP* matrix mender cells, except that their numbers peaked slightly higher
232 and two days later (compare Fig. 2G,H to Fig. 1L). Although the difference is explained
233 by nuclear RFP persisting longer than cytoplasmic GFP, it also indicates that matrix
234 menders persist after they turn off collagen expression. After the peak, the number of
235 RFP+ cells decreased rapidly. We expected that the RFP+ cells would transition into
236 GFP+ lineage cells, because enteroblasts can remain dormant for weeks before
237 differentiating into enterocytes in a healthy gut epithelium[28]. Contrary to our
238 expectations, however, as RFP+ cells disappeared, the corresponding pulse of GFP+
239 cells was much smaller (Fig. 2H). These results indicate that most matrix menders are
240 removed from the gut epithelium after repair is complete. Matrix menders are capable of
241 differentiating into enterocytes, however, as the enterocyte-specific antibody Pdm1
242 stained about 15% (50/340) of GFP+ lineage-expressing cells after 2 days recovery but
243 did not stain RFP+ collagen-expressing cells (Fig. S6F,G). Matrix menders never
244 became enteroendocrine cells, as no G-TRACE labeled cells were labeled with anti-
245 Prospero (Fig. S6E). To determine if some matrix menders were dying, we stained
246 *Cg>G-TRACE* flies with anti-Cleaved Caspase 3 (CC3). In vehicle-treated guts, we

247 found ~9% of RFP+ matrix mender cells were positive for the cell death marker (Fig.
248 S6H). In guts recovering from DSS damage, the percentage of dying matrix menders
249 increased over time: at 0 d post DSS, 5% were labeled as dying, but by 4 d post DSS
250 feeding (2 d recovery) 15% RFP+ cells were labeled as dying (Fig. 2I,J and Fig S6H).
251 Although kinetic analysis is limited in fixed samples, it appears that most matrix
252 menders do not differentiate into enterocytes and are short-lived, a property of
253 enteroblasts generally after DSS treatment (Fig. S6B)**.** Taken together, these results
254 indicate that as repair is completed, matrix menders first turn off collagen, then a few
255 differentiate while most die.
256

257 **Piezo is required for matrix menders to arise in response to damage.**

258 How does the gut sense damage to turn on Col4? Using a quantitative tensile
259 strain assay, we previously demonstrated that DSS damage makes basement
260 membranes less stiff (reduced elastic modulus)[14], and we envision that most types of
261 matrix damage would result in reduced stiffness (increased flexibility). Thus, we
262 reasoned that basement membrane damage might be detected by a mechanosensitive
263 mechanism such as the ion channel Piezo, known to be active in the fly gut[11,29,30]. To
264 test Piezo's role in basement membrane repair, we analyzed *Piezo*^{KO} null flies, which
265 are homozygous viable. After damaging with DSS, *Piezo*^{KO} flies were unable to repair
266 basement membranes (Fig. 3A-C), but unlike other matrix repair genes (Fig. S1), *Piezo*
267 was not required for basement membrane maintenance (Fig. 3 D-F). Analysis of a
268 second independent mutation, *Piezo*^{MI04294}*,* confirmed its unusual repair-specific
269 function (Fig. S7A-F). To determine if *Piezo* is required for detection of basement

270 membrane damage, we quantified Cg-expressing matrix mender cells in *Piezo*^{KO} versus
271 control midguts after DSS damage. Piezo was required for matrix mender induction: in
272 controls, 5.8% of epithelial cells were matrix menders, but in *Piezo*^{KO} only 1.9% were
273 and their *Cg* expression level was reduced (Fig. 3G-J). Thus, *Piezo* is required for
274 matrix menders to arise in response to damage.
275

276 **Piezo is expressed in a subset of intestinal stem cells.**

277 For Piezo to monitor basement membrane damage, it must be present prior to
278 damage. To localize Piezo, first we tried a functional GFP-Piezo fusion protein at the
279 endogenous locus reported to be extremely dim in neurons[31], but we were unable to
280 detect GFP in the gut. Next, we turned to a Gal4-based *Piezo>GFP* transcriptional
281 reporter, expressed outside the gut epithelium in tracheal cells that penetrate the gut
282 muscles (Fig. S7G,H) and in small cells within the gut epithelium. On regular food, 93%
283 of *Piezo>GFP* cells were positive for the intestinal stem cell marker Dl but only 36% of
284 Dl+ stem cells expressed Piezo (Fig. 2K-O). Our results are similar to a previous report
285 that *Piezo* is expressed in 40% of intestinal stem cells[11]. We found that stem cells are
286 often adjacent to matrix menders (Fig. 3P-Q), suggesting that stem cell divisions give
287 rise to matrix menders in a Piezo-dependent manner.
288

289 **Piezo detects decreased basement membrane stiffness to activate matrix**
290 **menders.**

291 What aspect of basement membrane damage does Piezo detect? Piezo is a
292 transmembrane channel activated by mechanical stretch to the plasma membrane[32],

293 and the plasma membranes of intestinal stem cells are in direct contact with the
294 underlying basement membrane[33]. A damage-induced loss of tensile stiffness in the
295 basement membrane is expected to put more tension on neighboring plasma
296 membranes, resulting in membrane stretching and Piezo activation. Thus, we
297 hypothesized that Piezo detects basement membrane damage via its loss of stiffness.
298 As a test, we specifically reduced basement membrane stiffness in otherwise healthy
299 and undamaged animals, by inhibiting the Col4 crosslinking enzyme Peroxidasin.
300 *Peroxidasin* mouse mutant tissue has reduced basement membrane stiffness (Young's
301 modulus), measured as increased deformation (stretch) in response to tension[18]. Using
302 the same quantitative tensile strain assay, we recently reported that inhibiting
303 Peroxidasin in wild-type adult *Drosophila* by feeding 100 μM of the suicide substrate
304 phloroglucinol (PHG) for 5 days decreases basement membrane stiffness by about
305 half[17]. The PHG-induced decrease in basement membrane stiffness was evident in the
306 muscle aspect ratio, both at 100 μM and even more strongly at 5 mM, indicating a dose
307 response (Fig. 7A-D). Excitingly, 100 μM PHG alone without other damage induced
308 matrix menders (3.5% of gut epithelial cells), and 5 mM PHG induced even more matrix
309 menders (5.3%), at a level similar to DSS induction (Fig. 4E,F,H, compare to Fig. 1L).
310 Thus, the loss of stiffness specifically activated matrix mender cells. Further, the
311 mechanical induction of matrix menders required *Piezo*, as PHG-induced matrix
312 menders were completely suppressed in the $Piezo^{KO}$ background (Fig. 4G,H). These
313 results indicate that Piezo responds to the reduction in basement membrane stiffness to
314 give rise to collagen-expressing matrix mender cells, positioned adjacent to the
315 basement membrane (Fig. 4I,J) where they can effect repair.
316

317 **Discussion**

318 Using the basement membrane around the *Drosophila* posterior midgut as an
319 experimental model, we found that basement membrane damage gives rise to and is
320 repaired by a distinct set of local epithelial cells, matrix mender cells, defined by their
321 expression of the Collagen IV reporter *Cg-Gal4*. Matrix mender cells supply Col4
322 specifically required for repair: when Col4a1 or Vkg is knocked down in these cells,
323 undamaged guts appear normal, but guts with basement membrane damage cannot
324 repair. Most matrix menders are transient: after basement membrane repair is
325 completed, matrix menders turn off collagen expression and most of them die. In
326 contrast, Col4 is a long-lived molecule that is difficult to dispose of once deposited, and
327 too much leads to fibrosis. Perhaps it is important to limit the duration of collagen-
328 generating cells so they cannot cause fibrosis, thus making a long-lived molecule from a
329 short-lived cell.

330 The matrix mender cells are a subset of enteroblasts, daughters of intestinal
331 stem cells and progenitors of enterocytes. They are recognized by enteroblast marker
332 *Su(H)GBE*, most sit next to an intestinal stem cell, and ~15% differentiate into
333 enterocytes. Supporting data for enteroblasts expressing Col4 come from mining
334 published RNA sequencing data from single gut nuclei: transcripts for both Col4
335 subunits, *Cg25C* and *Vkg*, were identified almost exclusively in cells called progenitors
336 of enterocytes (proECs), defined as a subset of enteroblasts; further, after DSS
337 treatment, the number of proECs expressing the collagen transcripts doubled, results
338 similar to our findings but using very different methods to identify collagen expression
339 and cell identity[34,35]. Not all enteroblasts are matrix menders: in undamaged guts, only
340 21% of enteroblasts or 1.8% of epithelial cells express collagen, generally at low levels.

341 After basement membrane damage, the numbers increase: intestinal stem cell divisions
342 generate more total enteroblasts, and a greater percentage of them express collagen
343 (43%), with the result that about 6% of total epithelial cells express collagen, generally
344 at higher levels.

345 How is matrix damage detected to give rise to matrix menders? Matrix menders
346 arise in response to three independent challenges, DSS, paraquat, and PHG. All three
347 damage the basement membrane as assayed by gut morphology; in contrast, matrix
348 menders do not arise in response to the DNA damaging agent bleomycin, which does
349 not appear to damage the basement membrane although it damages the epithelial layer
350 and initiates stem-cell mediated repair[23,36]. Although DSS causes nonspecific damage
351 to both cells and matrix in the gut epithelium, PHG is highly specific, reducing the
352 number of head-to-head Col4 covalent sulfilimine crosslinks[16,37] and decreasing
353 basement membrane stiffness in a tensile strain assay, meaning that the basement
354 membrane will stretch more (increased strain) in response to a given pulling force or
355 tension[14,17]. The gut is a mechanically active environment, and increased basement
356 membrane stretching would cause increased stretching of neighboring plasma
357 membranes in the gut epithelial monolayer, activating mechanical stretch receptors.
358 Indeed, we found that the mechanosensitive transmembrane ion channel Piezo is
359 required specifically for basement membrane repair. Although many genes are required
360 for basement membrane repair, including those encoding basement membrane
361 components Nidogen, Perlecan, Laminin, Collagen IV, Peroxidasin, and the Collagen
362 chaperone protein SPARC, these genes are not specific to repair, as they are also
363 required for basement membrane maintenance. In contrast, the mechanosensitive ion

364 channel Piezo is required for repair only, not maintenance, confirmed with two
365 independent mutations. Our data strongly support a model that Piezo detects reductions
366 in basement membrane stiffness and signals for the generation of matrix menders.
367 Interestingly, even without induced damage, a few cells express collagen at low
368 levels in the midgut epithelium. We expect that low levels of basement membrane
369 damage are intrinsic to gut physiology given the proximity of the gut to an unpredictable
370 external environment and the mechanical wear and tear of peristalsis, and this low level
371 of damage would induce a weak matrix-mender response. Our various control data
372 show that in undamaged conditions the number of matrix menders is somewhat
373 variable, consistent with stochastic low levels of matrix damage.
374
375 Simple model of basement membrane repair and its limitations
376 We and others found Piezo expression in intestinal stem cells, so our data are
377 consistent with a simple stem-cell based model of basement membrane repair:
378 intestinal stem cells directly monitor basement membrane stiffness, with matrix damage
379 allowing greater cell stretching, activating Piezo. As a cation channel, Piezo activation
380 increases intracellular calcium levels, and sustained cytoplasmic calcium is known to be
381 sufficient to induce intestinal stem cell proliferation[38,39]. Thus, stem cells give rise to
382 matrix menders that express and secrete Col4 locally, restoring the structure of the
383 basement membrane. Their job complete, these cells turn off collagen expression and
384 most of them die. Although our data support this attractive model, it remains unclear
385 where Piezo detects basement membrane stiffness. Piezo is expressed in Dl+ intestinal
386 stem cells, but its function there has not been demonstrated as we have not had

success with Piezo conditional knockdown (i.e. ubiquitous knockdown does not reproduce the mutant phenotype). Nevertheless, our data strongly support a two-part model: (1) mechanical surveillance of basement membrane stiffness by Piezo, which activates (2) repair mediated by local epithelial cells. Indeed, very recently it was shown that stiffness regulates mouse intestinal stem cells via Piezo[40], and this may represent part of the mechanism we show here. Our basement membrane repair model is likely to be generalizable to other tissues and animals, as Piezo and basement membrane components are all highly conserved as is the tissue architecture of basement membranes in close contact with epithelial cells.

Lead contact

Further information and requests for resources and reagents should be directed to and will be fulfilled by the lead contact, Andrea Page-McCaw (andrea.page-mccaw@vanderbilt.edu)

Materials availability

Any requests for resources and reagents should be directed to the lead contact.

Data and code availability

All original code is publicly available: https://github.com/mshutson/cell-shape-analysis

Acknowledgements

We thank K. Elkie Peebles, Kimberly LaFever, Jordyn Sanner Barr, Leah Caplan, and Junmin Hua for technical help, Sergei Boudko and Patrick Page-McCaw for discussions, and Barry Denholm, Bruce Edgar, Yuh Nung Jan, BDSC, VDRC, and Kyoto DSC for fly stocks. CNA35 recombinant monomer protein was a gift from Sergei Boudko, and anti-Pdm1 was a gift from Yang Xiaohang. Work was supported by NIGMS (R01GM137595 to A.P-M., and F31GM148021 to A.S.)

Author Contributions

AS: Conceptualization, methodology, validation, formal analysis, investigation, resources, writing and editing, visualization. MSH: Methodology, software. APM: Conceptualization, methodology, writing and editing, visualization, supervision, project administration.

Competing interests

The authors declare no competing interests.

Supplemental Information

Document S1. Figures S1-S7

429 **Figure Legends**

430 **Figure 1. "Matrix mender" gut cells upregulate Col4 after basement membrane**
431 **damage.**

432 **(A) Left: *Drosophila* midgut.** The gut tube is covered with peristalsis muscles
433 (magenta) wrapped in basement membrane (green). Underneath the muscle layer, the
434 gut monolayer epithelium (blue nuclei/DAPI) comprises absorptive enterocytes (blue),
435 stem cells (brown), enteroblasts (gray), and enteroendocrine cells (red), all sitting on
436 basement membrane continuous with that of the muscles (green). Scale bars, 10 μm.
437 **Right: DSS damage.** DSS (orange dots) is ingested, transported through the
438 enterocytes, and deposited in the underlying basement membrane where it fractures the
439 basement membrane making it less stiff, resulting in visibly dysmorphic muscles
440 (described in Howard et al, 2019). Basement membranes and muscle shapes are fully
441 repaired 2 days after DSS is removed. Both repair and maintenance of the basement
442 membrane require basement membrane components and regulators (see Fig. S1 and
443 Howard et al, 2019, for data). Scale bars, 10 μm.
444 **(B-G)** Collagen IV (Vkg) in the gut basement membrane comes from the fat body in
445 undamaged conditions. B depicts the experiment knocking down GFP of Vkg-GFP
446 specifically in the fat body with *c564-Gal4*, data in C (*en face* view). After DSS damage,
447 some gut Vkg-GFP came from another source (D,E). Each dot in E represents a gut.
448 Cross-sections (F,G) show the new Vkg source deposits Vkg-GFP between the
449 epithelium and the muscles. Full data set for fat-body knockdown and the specificity of
450 the *c564-Gal4* driver shown in Fig. S2.

451 **(H-K)** Col4 reporter *Cg>GFP* identified unknown cells that respond to DSS in the gut.
452 Anterior (left), posterior (right). Posterior R4 midgut is the focus of this study. Scale bar,
453 100 µm in H,J, scale bar, 20 µm in I,K.
454 **(L-M)** Collagen-expressing cells ("matrix menders") increased in number during
455 basement membrane damage, then decreased during repair (L). Shaded regions
456 represent SEM. 5-21 guts analyzed per timepoint and treatment, see Fig. S3A for
457 dataset. Significance by *t*-test. In addition to number, expression level increased after
458 DSS (M), see arrowheads in I,K. Each dot represents a gut. Mean +/- SEM, significance
459 by *t*-test.
460 **(N-Q)** Feeding bleomycin did not damage the basement membrane, as indicated by
461 muscle shape (N-P), even though it did cause DNA damage and stem cell proliferation
462 (see Fig. S3B,C). Bleomycin did not induce *Cg>GFP*+ matrix menders (Q). Mean +/-
463 SEM, significance by *t*-test. Scale bar, 10 µm.
464 **(R-U)** Feeding paraquat damaged the basement membrane, indicated by changes in
465 muscle shape aspect ratio (R-T). Paraquat induced *Cg>GFP*+ matrix menders (U).
466 Mean +/- SEM, significance by *t*-test. Scale bar, 10 µm.
467
468 **Figure 2. Matrix menders are a subset of enteroblasts that provide Col4**
469 **necessary for repair and are short-lived.**
470 **(A)** Lineage of gut epithelial cell types.
471 **(B)** Matrix menders (*Cg>GFP*, green) expressed an enteroblast marker (*Su(H)GBE-*
472 *lacZ,* magenta). Scale bar, 10 µm.

473 **(C)** In both damaged and undamaged conditions, nearly all matrix menders were
474 enteroblasts expressing *Su(H)GBE-lacZ*, but not all enteroblasts were matrix menders
475 expressing *Cg>GFP*. After damage, more enteroblasts expressed *Cg>GFP*, evaluated
476 by Fisher's exact test. Number of cells scored is indicated.
477 **(D)** Total enteroblasts increased in response to DSS, SEM indicated. Each dot
478 represents 5-19 guts. Complete dataset in Fig. S6A.
479 **(E)** Repair required Col4 expressed from enteroblasts. *Col4a1* was knocked down in
480 different tissues, and adult gut muscle shape was compared in damaged-and-repaired
481 guts to unchallenged guts. When Col4a1 was fully expressed (first two columns), nearly
482 all guts had undamaged healthy basement membranes, both unchallenged and after
483 repair. Col4 from the fat body was required for development and/or homeostasis, as
484 guts appeared damaged even without challenge. Enteroblast Col4 was required
485 specifically for repair. Col4 was not required from enterocytes. Numbers of guts
486 evaluated is shown at column base. Guts were scored blinded to sample identity.
487 Knock-down in other gut cell types and knockdown of *vkg* confirmed that Col4 is
488 specifically required from enteroblasts for repair, see Fig. S5A-C. Significance evaluated
489 by Fisher's exact test.
490 **(F-H)** Dynamics of matrix mender cells during and after collagen expression determined
491 by G-TRACE. Overview (F) adapted from Evans et al., 2009. G, DSS increased the
492 number of real-time *Cg*-expressing cells (RFP+, magenta); after repair, *Cg*-expressing
493 RFP+ cells declined quickly, but most did not transition into lineage traced GFP+ cells
494 (green). Cells expressing both RFP+ and GFP+ were counted only as RFP+ (magenta)
495 to count each cell only once. Complete dataset in Fig. S6C,D.

496 **I,J)** *Cg>GTRACE* real-time expressing cells (RFP+, magenta) underwent cell death,
497 expressing Cleaved Caspase 3. Cell death of Cg-expressing cells was also observed
498 without DSS, see Fig. S6G. Shading represents SEM in G,H,J.
499
500 **Figure 3. Piezo is required for basement membrane repair and for matrix menders**
501 **to arise and is expressed in the intestinal stem cells.**
502 **(A-F)** *Piezo* was required for basement membrane repair but not maintenance in adult
503 guts. See Fig. S7A-F for confirmation with another allele. Mean +/-SEM. Significance by
504 *t-test*. Scale bar in B for A-E, 10 µm.
505 **(G-J)** *Piezo* was required for *Cg>GFP* matrix mender cells to arise in response to DSS
506 damage. Both the number and expression level of *Cg>GFP* cells were significantly
507 reduced in $Piezo^{KO}$ flies. Each dot represents a gut (I,J). Mean +/-SEM. Significance by
508 ANOVA (I) and *t*-test (J). Scale bar, 20 µm.
509 **(K-O)** Piezo-transcriptional reporter ($Piezo^{KI}$-*Gal4*, green) was expressed in Dl+
510 intestinal stem cells (magenta), flies fed normal food. Almost all Piezo+ cells were
511 Delta+ intestinal stem cells, yet only 36% of Dl+ intestinal stem cells express Piezo. For
512 Venn diagram, the circle size and amount of overlap are representative. Scale bars, 10
513 µm in K, 5 µm in L.
514 **(P-Q)** *Cg>GFP* matrix mender cells (green) were adjacent to intestinal stem cells (anti-
515 Delta, magenta). Scale bar, 10 µm. The number of cells analyzed is reported at column
516 base for M,N,Q.
517
518

519 **Figure 4. Piezo detects decreases in basement membrane stiffness to activate**
520 **matrix menders.**
521 **(A)** PHG inhibits collagen IV crosslinking enzyme Pxn.
522 **(B-D)** Feeding PHG reduced basement membrane stiffness in a dose-dependent
523 manner, evidenced by muscle aspect ratio. Quantitative tensile stiffness measurements
524 were reported in Peebles et. al., (2024). Significance evaluated by ANOVA. Mean +/-
525 SEM. Scale bar, 10 μm.
526 **(E-F)** Reducing collagen crosslinking induced matrix mender cells. Scale bar, 20 μm.
527 **(G-H)** Piezo was required for matrix mender cells to arise in response to reduced
528 collagen crosslinking. Each data point represents an individual gut. Mean +/-SEM.
529 Significance by ANOVA.
530 **(I-J)** Matrix mender cells have extensive contact with basement membrane, both with
531 and without DSS (no recovery), positioning them well to repair it. Collagen is labeled
532 with the triple-helix binding protein, CNA35 (green). Scale bar, 10 μm.
533

534 ## Materials and Methods

535 **Key resources table**

REAGENT or RESOURCE	SOURCE	IDENTIFIER
Antibodies		
Mouse anti-β gal	Developmental Studies Hybridoma Bank	Cat# 40-1a; RRID:AB_528100
Rabbit anti-Cleaved Caspase 3	Cell Signaling Technology	Cat# 9661; RRID:AB_2341188
Mouse anti-Delta	Developmental Studies Hybridoma Bank	Cat# SA4; RRID:AB_2056641
Rabbit anti-H2AvD	Rockland	Cat# 600-401-914; RRID:AB_828383
Rabbit anti-pH3	Millipore	Cat# 06-570; RRID:AB_310177
Mouse anti-Prospero	Developmental Studies Hybridoma Bank	Cat# MR1A; RRID:AB_528440
Rabbit anti-Pdm1	Yang Xiaohang	n/a
Cy3 goat anti-mouse IgG1	Jackson ImmunoResearch Labs	Cat# 115-165-205; RRID:AB_2338694
Cy3 donkey anti-rabbit IgG	Jackson ImmunoResearch Labs	Cat# 711-165-152; RRID:AB_2307443
Cy5 goat anti-mouse IgG	Jackson ImmunoResearch Labs	Cat# 115-175-205; RRID:AB_2338715
Cy5 donkey anti-rabbit	Jackson ImmunoResearch Labs	Cat# 711-175-152; RRID:AB_2340607
Experimental models: Organisms/strains		
D. melanogaster: VkgGFP^{791}: *y w; vkgP{GFP791, w+}*	Carnegie Protein trap library via Sally Horne-Badovinac	CC00791
UAS-GFP^{RNAi}: *w[1118]; P{w[+mC]=UAS-GFP.RNAi.R}142*	Bloomington Drosophila Stock Center	9330
VkgGFP, UAS-GFP^{RNAi}/CyO, mCh	this study	n/a
Cg-Gal4: *w[1118]; P{w[+mC]=Cg-GAL4.A}2*	Bloomington Drosophila Stock Center	7011
UAS-GFP: *w[*]; P{w[+mC]=UAS-GFP.S65T}eg[T10]*	Bloomington Drosophila Stock Center	1522
Su(H)GBE-lacZ: *w[*]; l(2)*[*]/CyO, P{ry[+t7.2]=en1}wg[en11];* *P{ry[+t7.2]=Ddc.E(spl)m8-HLH-lacZ.Gbe}3*	Bloomington Drosophila Stock Center	83352
Su(H)GBE-Gal4, UAS-mCD8GFP: *w[*]; P{w[+mC]=Su(H)GBE-GAL4}2, P{w[+mC]=UAS-mCD8::GFP.L}LL5, P{UAS-mCD8::GFP.L}2/CyO*	Bloomington Drosophila Stock Center	83377

UAS-Cg25c^{RNAi} *w1118; P{GD12784}v28369*	Vienna Drosophila Resource Center	28369
VkgRNAi (RNAi #1): *P{KK111668}VIE-260B*	Vienna Drosophila Resource Center	106812
VkgRNAi (RNAi #2): *y[1] v[1]; P{y[+t7.7] v[+t1.8]=TRiP.HMC02400}attP2*	Bloomington Drosophila Stock Center	50895
c564-Gal4: *w[1118]; P{w[+mW.hs]=GawB}c564*	Bloomington Drosophila Stock Center	6982
Myo1a-Gal4: *w*; P{w+mW.hs=GawB}NP0001 / CyO, P{w-=UAS-lacZ.UW14}UW14*	Drosophila Genomics Resource Center	112001
UAS-GTRACE: *w[*]; P{w[+mC]=UAS-RedStinger}6, P{w[+mC]=UAS-FLP.Exel}3, P{w[+mC]=Ubi-p63E(FRT.STOP)Stinger}15F2*	Bloomington Drosophila Stock Center	28281
Piezo^{KO}: *w[*]; PBac{w[+mC]=RB5.WH5}Piezo[KO]*	Bloomington Drosophila Stock Center	58770
Piezo^{KO}, VkgGFP^{791}	this study	n/a
Piezo^{KO}, Cg-Gal4/CyO	this study	n/a
Piezo^{KO}; UAS-GFP/TM3	this study	n/a
Piezo^{KI}-Gal4: *w[*]; TI{GAL4}Piezo[KI]*	Bloomington Drosophila Stock Center	78335
UAS-myr-RFP: *w[*]; P{w[+mC]=Cg-GAL4.A}2, P{w[+mC]=UAS-myr-mRFP}1/CyO; P{w[+mC]=UAS-GFP.RNAi.R}142*	Bloomington Drosophila Stock Center	63147
VkgGFP^{791}; tubGal4, tubGal80^{ts}/S-T	this study	n/a
UAS-Perlecan^{RNAi} (RNAi #1): *P{KK110494}VIE-260B*	Vienna Drosophila Resource Center	108157
UAS-Perlecan^{RNAi} (RNAi #2): *y[1] v[1]; P{y[+t7.7] v[+t1.8]=TRiP.GL01153}attP2*	Bloomington Drosophila Stock Center	42783
UAS-Nidogen^{RNAi} (RNAi #1): *y[1] v[1]; P{y[+t7.7] v[+t1.8]=TRiP.HMJ24142}attP40/CyO*	Bloomington Drosophila Stock Center	62902
UAS-Nidogen^{RNAi} (RNAi #2): *P{KK109625}VIE-260B*	Vienna Drosophila Resource Center	102310
UAS-SPARC^{RNAi} (RNAi #1): *P{KK100566}VIE-260B*	Vienna Drosophila Resource Center	103707
UAS-SPARC^{RNAi} (RNAi #2): *y[1] v[1]; P{y[+t7.7] v[+t1.8]=TRiP.HMS02133}attP40*	Bloomington Drosophila Stock Center	40885
UAS-Gbp1^{RNAi}: *P{KK110262}VIE-260B*	Vienna Drosophila Resource Center	108755
UAS-Gbp2^{RNAi}: *w[1118]; P{GD4931}v16696*	Vienna Drosophila Resource Center	16696
Pxn-Gal4/TM3: *y[1] w[67c23]; Mi{GFP[E.3xP3]=ET1}Pxn[MB00459]*	Bloomington Drosophila Stock Center	22805
LanB1-Gal4/CyO: *w[1118]; PBac{w[+mC]=IT.GAL4}LanB1[0987-G4]/CyO*	Bloomington Drosophila Stock Center	63941

Tubulin-Gal4: *y[1] w[*]; P{w[+mC]=tubP-GAL4}LL7/TM3, Sb[1] Ser[1]*	Bloomington Drosophila Stock Center	5138
Prospero-Gal4: *w[*]; P{w[+mC]=GAL4-pros.MG}3*	Bloomington Drosophila Stock Center	80572
Btl-Gal4	Greg Beitel	FBti0148919
TubGal80ts/CyO; DlGal4/TM6B	Bruce Edgar	FBal0256627
Piezo^{MI0429}: *y[1] w[*]; Mi{y[+mDint2]=MIC}Piezo[MI04294]*	Bloomington Drosophila Stock Center	37433
Oligonucleotides		
PCR *Piezo^{KO} F:* GAGTGAGCTGATACCGCTCGC	this study	n/a
PCR *Piezo^{KO} R:* CAGCGACGGATTCGCGC	this study	n/a
Software and algorithms		
ImageJ 1.53v	National Institutes of Health	https://imagej.net/software/fiji/
Graphpad Prism 9.5		https://www.graphpad.com/
Seedwater Segmenter	Mashburn et al. 2012	n/a
Mathematica	Wolfram Inc.	https://github.com/mshutson/cell-shape-analysis

Fly husbandry

Flies were maintained on cornmeal-molasses food at 25 °C unless otherwise specified. Adult-onset RNAi-based gene knockdown was done under *Gal80^{ts}* control, with flies maintained at 18 °C until they eclosed. Female flies were then aged at 18 °C until they were 6-day adults (mated) before moving them to 29 °C to activate Gal4. Each experiment contains data from at least two independent crosses. For the list of fly stocks, please refer to Key Resource Table.

Confirming *Piezo^{KO}* using PCR

Because *Piezo^{KO}* flies have no obvious phenotype, we verified the presence of the deletion by PCR in the starting stock and in recombinants. Primers were designed and optimized against the Piggybac insertion PBac{WH}CG8486-f02291 in *Piezo^{KO}* animals to confirm the loss of Piezo using the following primers – F:

550 GAGTGAGCTGATACCGCTCGC, R: CAGCGACGGATTCGCGC. OneTaq2x Master
551 Mix with standard buffer was used. The following PCR conditions were used – Initial
552 Denaturation: 94 °C, 30 sec; denaturation: 94 °C, 30 sec; annealing: 65 °C, 60 sec;
553 extension: 68 °C, 45 sec (30x cycles); final extension: 68 °C, 5 minutes.
554

555 **DSS feeding**

556 All DSS feeding experiments used mated female flies aged 3-5 d after eclosion
557 before feeding DSS. Flies utilizing the *Gal80^{ts}* system were moved to 29 °C for 2 days to
558 ensure the Gal4 was active prior to starting DSS feeding treatments. Flies not utilizing
559 the Gal80^{ts} system were aged 3-5 days at 25 °C prior to starting DSS feeding
560 treatments. DSS was administered as described in Amcheslavsky et al. (2009) and
561 Howard et al. (2019): a 2.5 cm x 3 cm piece of chromatography paper (Whatman 3030-
562 861, Grade 3 MM CHR) was placed in an empty vial. 500 µl of a 5% sucrose solution
563 with or without 3% 36-50 kDa DSS (dextran sulfate sodium salt colitis grade, MP
564 Biomedicals, CAS number 9011-18-1, 36,000 – 50,000 MW) was added to the paper in
565 the vial. Female flies were anesthetized and carefully placed in the vial. Flies were
566 added to new vials with fresh media each day for 2 days. For recovery experiments,
567 flies were transferred to a vial containing standard cornmeal-molasses food for 2 days.
568 For imaging in 3 dimensions (Z-stacks), flies on standard cornmeal-molasses food were
569 fed 5% sucrose for 4 hours before dissection to reduce gut autofluorescence from the
570 food.
571

572 **Phloroglucinol feeding**

573 PHG was fed to flies by dissolving it in food prepared without any cornmeal,
574 freshly made with or without 100 μM or 5 mM Phloroglucinol (PHG) (Sigma-Aldrich,
575 CAS number 108-73-6) and solidified in a vial overnight. 20 aged female flies and 5
576 male flies were added to the vials with or without PHG. Flies were kept at 25 °C for 5
577 days. Prior to dissection, flies were fed 5% sucrose for 4 hours before dissection to
578 reduce gut autofluorescence from the food.
579

580 **Bleomycin feeding**

581 Bleomycin (Sigma, 9041-93-4) was dissolved in water at a final concentration of
582 25 μg/mL and 5% sucrose, or 5% sucrose as a control. 500 μl of bleomycin or control
583 solution were added to a 2.5 cm x 3 cm piece of chromatography paper at the bottom of
584 an empty food vial. Flies were fed bleomycin for 2 days, changing the filter paper and
585 vial daily.
586

587 **Paraquat feeding**

588 A 10 mM paraquat (Sigma, 75365-73-0) solution was made in water with 5%
589 sucrose, or 5% sucrose alone as the control. Flies were starved in an empty vial for 4
590 hours before transferring them to a vial with a 2.5 cm x 3 cm piece of chromatography
591 paper soaked with either 500 μl of paraquat or control solution. Flies were fed for 16
592 hours prior to dissection.
593

594 **Gut dissections and preparations**

595 Adult females were placed in cold Grace's media and pinched between the
596 abdomen and thorax using sharp #5 dissecting forceps (Dumont). The abdomen was
597 separated from the thorax, and the integument surrounding the abdomen was peeled
598 away, exposing the gut and Malpighian tubules, being careful not to pinch or stretch the
599 gut. The Grace's media was removed using a Pasteur pipette, followed by one quick
600 wash with 1x PBS (137 mM NaCl, 2.7 mM KCl, 10 mM Na_2HPO_4, and 1.8 mM KH_2PO_4).
601 The guts were fixed with 8% paraformaldehyde (Ted Pella, Paraformaldehyde 16%,
602 Product #18505) in PBS for 60 minutes at room temperature, followed by 3 quick
603 washes in PBS, and 4 x 15 min washes with PBS or PBT.
604 For immunofluorescence experiments, blocking buffer was added to fixed guts
605 for 2 hours at room temperature or overnight at 4 °C then incubated in primary antibody
606 and 0.2 µM SiRActin (Spirochrome Cat# SC001) in PBS or PBT overnight at 4 °C,
607 followed by 4 x 30 min washes with 1x PBS. Secondary antibodies were added for 2
608 hours at room temperature, followed by 4 x 30 min washes. Guts were then mounted in
609 DAPI-containing mounting media (Vectashield, Vector Laboratories, H1200). Antibodies
610 used were mouse anti-β gal (1:50), rabbit anti-Cleaved Caspase 3 (1:200), mouse anti-Delta
611 (1:50), rabbit anti-H2AvD (1:1000), rabbit anti-pH3 (1:1000), mouse anti-Prospero (1:50), and
612 rabbit anti-Pdm1 (1:1000). The following secondary antibodies were used at 1:200 Cy3 goat
613 anti-mouse IgG1, Cy3 donkey anti-rabbit IgG, Cy5 goat anti-mouse IgG, and Cy5 donkey anti-
614 rabbit.
615

616 **CNA35 staining**

617 Immediately after gut dissections, CNA35 recombinant monomer protein labeled
618 with Alexa488 (1 mg/ml in PBS) was diluted to 1:100 in PBS and added to guts for 2
619 hours, followed by 1 quick wash in PBS and fixed for 1 hour with 8% PFA.
620

621 **Light Microscopy**

622 Single optical sections of the posterior midgut (R4) were imaged using a Zeiss
623 Apotome mounted to an Axio Image M2 with a 63x/1.4 oil Plan-Apochromat objective.
624 Z-stacks were acquired using a 40x/1.3 oil Plan-Apochromat objective at a 0.75 μm step
625 size taken through the top half of the gut tube (lumen through the top of the muscle
626 layer). Images were taken using an AxioCam MRm camera (Zeiss), X-Cite 120Q light
627 source (Excelitas Technologies), and AxioVision 4.8 software. FIJI ImageJ (version
628 1.53v, National Institutes of Health) 16-bit, ZVI files were used for analysis and figures
629 for images.

630 For Fig 1C,D and Fig S2A-H, the fluorescence intensity of the basement
631 membrane was determined by taking single optical slices *en face* through the middle of
632 the circumferential muscles to ensure the same plane of the basement membrane was
633 imaged, and the exposures were kept the same. The fluorescence intensity of the
634 basement membrane was measured in ImageJ using the “box” tool to measure the
635 average intensity of 3 representative regions of the gut basement membrane. Similarly,
636 the background intensity was determined by subtracting the average of 3 boxes outside
637 of the gut region. An AVOVA test was performed (GraphPad Prism 9.5).

638 Fluorescence intensity measurements of gut cells to be compared were acquired
639 at the same exposure from at least 3 experiments done on different days. Maximum

640 intensity projections were created using FIJI ImageJ and the line tool was used to draw
641 through the center of the 3 brightest nuclei in the GFP channel and the fluorescence
642 intensity was measured and averaged. Background fluorescence was subtracted by
643 taking the average intensity of 3 lines within the gut region that did not overlap with GFP
644 nuclei. An unpaired *t-test* was performed.
645

646 **Measurement of muscle shape**

647 Using single-slice cross section images of the gut basement membrane,
648 individual muscle cells were identified and segmented using the software Seedwater
649 Segmenter (Mashburn et al. 2012). Custom code in Mathematica (Wolfram Inc.,
650 Champaign, IL) was then used to analyze the segmented images and determine the
651 aspect ratio of each muscle cell (code available at https://github.com/mshutson/cell-
652 shape-analysis). Specifically, to quantify the aspect ratio of gut muscle cells, we first fit a
653 4th-order polynomial to all the segmented cells to estimate a tangent line along the gut's
654 long axis. We then calculated the two-dimensional moment-of-inertia tensor, J, for each
655 cell relative to the local tangent line, and calculated each cell's aspect ratio as
656 Sqrt[J11/J22]. This aspect ratio is thus the cell's height normal to the gut's long axis
657 divided by the cell's length along the gut's long axis.
658

659 **Quantifying number of cells**

660 GFP+ cells were manually quantified by creating a maximum intensity projection
661 of the Z-stack images of the top half of the gut and confirmed by the presence of a
662 nucleus. The total number of nuclei in the posterior midgut was quantified by creating a
663 maximum intensity projection and setting a threshold to select the DAPI-stained nuclei.

664 Images were “despeckled,” and a watershed was applied to the image. Using the
665 ImageJ “analyze particle” feature, the number of particles larger than 5 μm^2 was
666 quantified. The areas where nuclei were fused together or unable to be accurately
667 quantified by ImageJ were manually quantified. The total number of GFP+ cells
668 captured in each image was divided by the total number of nuclei in the image and
669 multiplied by 100 to report the #GFP cells/100.
670
671 **Statistical reporting**
672 All statistical analysis was performed using GraphPad Prism 9.5. ns indicates $P > 0.05$, * indicates $P \leq 0.05$, ** indicates $P \leq 0.01$, *** indicates $P \leq 0.001$, **** indicates $P \leq 0.0001$.
673
674
675

676 **References**

677 1. Iozzo, R.V., and Gubbiotti, M.A. (2018). Extracellular matrix: The driving force of
678 mammalian diseases. Matrix Biology *71–72*, 1–9.
679 https://doi.org/10.1016/j.matbio.2018.03.023.

680 2. Bonnans, C., Chou, J., and Werb, Z. (2014). Remodelling the extracellular matrix in
681 development and disease. Nat Rev Mol Cell Biol *15*, 786–801.
682 https://doi.org/10.1038/nrm3904.

683 3. Liu, P., Xie, X., and Jin, J. (2020). Isotopic Nitrogen-15 Labeling of Mice Identified
684 Long-lived Proteins of the Renal Basement Membranes. Scientific Reports *10*, 1–7.
685 https://doi.org/10.1038/s41598-020-62348-6.

686 4. Verzijl, N., DeGroot, J., Thorpe, S.R., Bank, R.A., Shaw, J.N., Lyons, T.J., Bijlsma,
687 J.W.J., Lafeber, F.P.J.G., Baynes, J.W., and TeKoppele, J.M. (2000). Effect of
688 Collagen Turnover on the Accumulation of Advanced Glycation End Products.
689 Journal of Biological Chemistry *275*, 39027–39031.
690 https://doi.org/10.1074/jbc.M006700200.

691 5. Maroudas, A., Palla, G., and Gilav, E. (1992). Racemization of Aspartic Acid in
692 Human Articular Cartilage. Connective Tissue Research *28*, 161–169.
693 https://doi.org/10.3109/03008209209015033.

694 6. Sivan, S.-S., Wachtel, E., Tsitron, E., Sakkee, N., van der Ham, F., DeGroot, J.,
695 Roberts, S., and Maroudas, A. (2008). Collagen Turnover in Normal and
696 Degenerate Human Intervertebral Discs as Determined by the Racemization of
697 Aspartic Acid. Journal of Biological Chemistry *283*, 8796–8801.
698 https://doi.org/10.1074/jbc.M709885200.

699 7. Yurchenco, P.D., and Furthmayr, H. (1984). Self-Assembly of Basement Membrane
700 Collagen. Biochemistry *23*, 1839–1850. https://doi.org/10.1021/bi00303a040.

701 8. Fidler, A.L., Vanacore, R.M., Chetyrkin, S.V., Pedchenko, V.K., Bhave, G., Yin, V.P.,
702 Stothers, C.L., Rose, K.L., McDonald, W.H., Clark, T.A., et al. (2014). A unique
703 covalent bond in basement membrane is a primordial innovation for tissue evolution.
704 Proceedings of the National Academy of Sciences of the United States of America
705 *111*, 331–336. https://doi.org/10.1073/pnas.1318499111.

706 9. Ramos-Lewis, W., and Page-McCaw, A. (2019). Basement membrane mechanics
707 shape development: Lessons from the fly. Matrix Biology *75–76*, 72–81.
708 https://doi.org/10.1016/j.matbio.2018.04.004.

709 10. Buszczak, M., Paterno, S., Lighthouse, D., Bachman, J., Planck, J., Owen, S.,
710 Skora, A.D., Nystul, T.G., Ohlstein, B., Allen, A., et al. (2007). The Carnegie Protein
711 Trap Library: A Versatile Tool for Drosophila Developmental Studies. Genetics *175*,
712 1505–1531. https://doi.org/10.1534/genetics.106.065961.

713 11. He, L., Si, G., Huang, J., Samuel, A.D.T., and Perrimon, N. (2018). Mechanical
714 regulation of stem cell differentiation through stretch-activated Piezo channel.
715 Nature *555*, 103–106. https://doi.org/10.1038/nature25744.

716 12. Martin, J.L., Sanders, E.N., Moreno-Roman, P., Koyama, L.A.J., Balachandra, S.,
717 Du, X., and O'Brien, L.E. (2018). Long-term live imaging of the Drosophila adult
718 midgut reveals real-time dynamics of division, differentiation and loss. eLife *7*.
719 https://doi.org/10.7554/ELIFE.36248.

720 13. Micchelli, C.A., and Perrimon, N. (2006). Evidence that stem cells reside in the adult
721 Drosophila midgut epithelium. Nature *439*, 475–479.
722 https://doi.org/10.1038/nature04371.

723 14. Howard, A.M., Lafever, K.S., Fenix, A.M., Scurrah, C.R., Lau, K.S., Burnette, D.T.,
724 Bhave, G., Ferrell, N., and Page-McCaw, A. (2019). DSS-induced damage to
725 basement membranes is repaired by matrix replacement and crosslinking. Journal
726 of Cell Science *132*. https://doi.org/10.1242/jcs.226860.

727 15. Shimshoni, E., Adir, I., Afik, R., Solomonov, I., Shenoy, A., Adler, M., Puricelli, L.,
728 Sabino, F., Savickas, S., Mouhadeb, O., et al. (2021). Distinct extracellular–matrix
729 remodeling events precede symptoms of inflammation. Matrix Biology *96*, 47–68.
730 https://doi.org/10.1016/j.matbio.2020.11.001.

731 16. McCall, A.S., Cummings, C.F., Bhave, G., Vanacore, R., Page-Mccaw, A., and
732 Hudson, B.G. (2014). Bromine is an essential trace element for assembly of
733 collagen IV scaffolds in tissue development and architecture. Cell *157*, 1380–1392.
734 https://doi.org/10.1016/j.cell.2014.05.009.

735 17. Peebles, K.E., LaFever, K.S., Page-McCaw, P.S., Colon, S., Wang, D., Stricker,
736 A.M., Ferrell, N., Bhave, G., and Page-McCaw, A. (2024). Peroxidasin is required for
737 full viability in development and for maintenance of tissue mechanics in adults.
738 Matrix Biology *125*, 1–11. https://doi.org/10.1016/j.matbio.2023.11.005.

739 18. Bhave, G., Colon, S., and Ferrell, N. (2017). The sulfilimine cross-link of collagen IV
740 contributes to kidney tubular basement membrane stiffness. American Journal of
741 Physiology - Renal Physiology *313*, F596–F602.
742 https://doi.org/10.1152/ajprenal.00096.2017.

743 19. O'Connor, J.T., Stevens, A.C., Shannon, E.K., Akbar, F.B., LaFever, K.S.,
744 Narayanan, N.P., Gailey, C.D., Hutson, M.S., and Page-McCaw, A. (2021).
745 Proteolytic activation of Growth-blocking peptides triggers calcium responses
746 through the GPCR Mthl10 during epithelial wound detection. Developmental Cell *56*,
747 2160-2175.e5. https://doi.org/10.1016/j.devcel.2021.06.020.

748 20. Pastor-Pareja, J.C., and Xu, T. (2011). Shaping Cells and Organs in Drosophila by
749 Opposing Roles of Fat Body-Secreted Collagen IV and Perlecan. Developmental
750 Cell *21*, 245–256. https://doi.org/10.1016/j.devcel.2011.06.026.

751 21. Ramos-Lewis, W., LaFever, K.S., and Page-McCaw, A. (2018). A scar-like lesion is
752 apparent in basement membrane after wound repair in vivo. Matrix Biology *74*, 101–
753 120. https://doi.org/10.1016/j.matbio.2018.07.004.

754 22. Asha, H., Nagy, I., Kovacs, G., Stetson, D., Ando, I., and Dearolf, C.R. (2003).
755 Analysis of Ras-Induced Overproliferation in Drosophila Hemocytes. Genetics *163*,
756 203–215. https://doi.org/10.1093/genetics/163.1.203.

757 23. Amcheslavsky, A., Jiang, J., and Ip, Y.T. (2009). Tissue Damage-Induced Intestinal
758 Stem Cell Division in Drosophila. Cell Stem Cell *4*, 49–61.
759 https://doi.org/10.1016/j.stem.2008.10.016.

760 24. Choi, N.H., Kim, J.G., Yang, D.J., Kim, Y.S., and Yoo, M.A. (2008). Age-related
761 changes in Drosophila midgut are associated with PVF2, a PDGF/VEGF-like growth
762 factor. Aging Cell *7*, 318–334. https://doi.org/10.1111/j.1474-9726.2008.00380.x.

763 25. Buchon, N., Broderick, N.A., Poidevin, M., Pradervand, S., and Lemaitre, B. (2009).
764 Drosophila Intestinal Response to Bacterial Infection: Activation of Host Defense
765 and Stem Cell Proliferation. Cell Host & Microbe *5*, 200–211.
766 https://doi.org/10.1016/j.chom.2009.01.003.

767 26. Furriols, M., and Bray, S. (2001). A model Notch response element detects
768 Suppressor of Hairless–dependent molecular switch. Current Biology *11*, 60–64.
769 https://doi.org/10.1016/S0960-9822(00)00044-0.

770 27. Evans, C.J., Olson, J.M., Ngo, K.T., Kim, E., Lee, N.E., Kuoy, E., Patananan, A.N.,
771 Sitz, D., Tran, P.T., Do, M.T., et al. (2009). G-TRACE: Rapid Gal4-based cell
772 lineage analysis in Drosophila. Nature Methods *6*, 603–605.
773 https://doi.org/10.1038/nmeth.1356.

774 28. Antonello, Z.A. (2015). Robust intestinal homeostasis relies on cellular plasticity in
775 enteroblasts mediated by miR-8–Escargot switch. The EMBO Journal *34*, 2025–
776 2041. https://doi.org/10.15252/embj.201591517.

777 29. Min, S., Oh, Y., Verma, P., Whitehead, S.C., Yapici, N., Van Vactor, D., Suh, G.S.B.,
778 and Liberles, S.D. (2021). Control of feeding by piezo-mediated gut
779 mechanosensation in Drosophila. eLife *10*, 1–30.
780 https://doi.org/10.7554/eLife.63049.

781 30. Lee, J., Cabrera, A.J.H., Nguyen, C.M.T., and Kwon, Y.V. (2020). Dissemination of
782 Ras V12-transformed cells requires the mechanosensitive channel Piezo. Nature
783 Communications *11*, 1–13. https://doi.org/10.1038/s41467-020-17341-y.

784 31. Song, Y., Li, D., Farrelly, O., Miles, L., Li, F., Kim, S.E., Lo, T.Y., Wang, F., Li, T.,
785 Thompson-Peer, K.L., et al. (2019). The Mechanosensitive Ion Channel Piezo
786 Inhibits Axon Regeneration. Neuron *102*, 373-389.e6.
787 https://doi.org/10.1016/j.neuron.2019.01.050.

32. Coste, B., Mathur, J., Schmidt, M., Earley, T.J., Ranade, S., Petrus, M.J., Dubin, A.E., and Patapoutian, A. (2010). Piezo1 and Piezo2 Are Essential Components of Distinct Mechanically Activated Cation Channels. Science *330*, 55–60. https://doi.org/10.1126/science.1193270.

33. You, J., Zhang, Y., Li, Z., Lou, Z., Jin, L., and Lin, X. (2014). Drosophila Perlecan Regulates Intestinal Stem Cell Activity via Cell-Matrix Attachment. Stem Cell Reports *2*, 761–769. https://doi.org/10.1016/j.stemcr.2014.04.007.

34. Petsakou, A., Liu, Y., Liu, Y., Comjean, A., Hu, Y., and Perrimon, N. (2023). Cholinergic neurons trigger epithelial Ca2+ currents to heal the gut. Nature, 1–3. https://doi.org/10.1038/s41586-023-06627-y.

35. single-cell RNA-seq data portal https://www.flyrnai.org/scRNA/gut_homeostasis_recovery/.

36. Tian, A., Wang, B., and Jiang, J. (2017). Injury-stimulated and self-restrained BMP signaling dynamically regulates stem cell pool size during Drosophila midgut regeneration. Proceedings of the National Academy of Sciences *114*. https://doi.org/10.1073/pnas.1617790114.

37. Bhave, G., Cummings, C.F., Vanacore, R.M., Kumagai-Cresse, C., Ero-Tolliver, I.A., Rafi, M., Kang, J.S., Pedchenko, V., Fessler, L.I., Fessler, J.H., et al. (2012). Peroxidasin forms sulfilimine chemical bonds using hypohalous acids in tissue genesis. Nature Chemical Biology *8*, 784–790. https://doi.org/10.1038/nchembio.1038.

38. Deng, H., Gerencser, A.A., and Jasper, H. (2015). Signal integration by Ca2+ regulates intestinal stem-cell activity. Nature *528*, 212–217. https://doi.org/10.1038/nature16170.

39. Xu, C., Luo, J., He, L., Montell, C., and Perrimon, N. (2017). Oxidative stress induces stem cell proliferation via TRPA1/RyR-mediated Ca2+ signaling in the Drosophila midgut. eLife *6*, e22441. https://doi.org/10.7554/eLife.22441.

40. Baghdadi, M.B., Houtekamer, R.M., Perrin, L., Rao-Bhatia, A., Whelen, M., Decker, L., Bergert, M., Pérez-Gonzàlez, C., Bouras, R., Gropplero, G., et al. (2024). PIEZO-dependent mechanosensing is essential for intestinal stem cell fate decision and maintenance. Science *386*, eadj7615. https://doi.org/10.1126/science.adj7615.

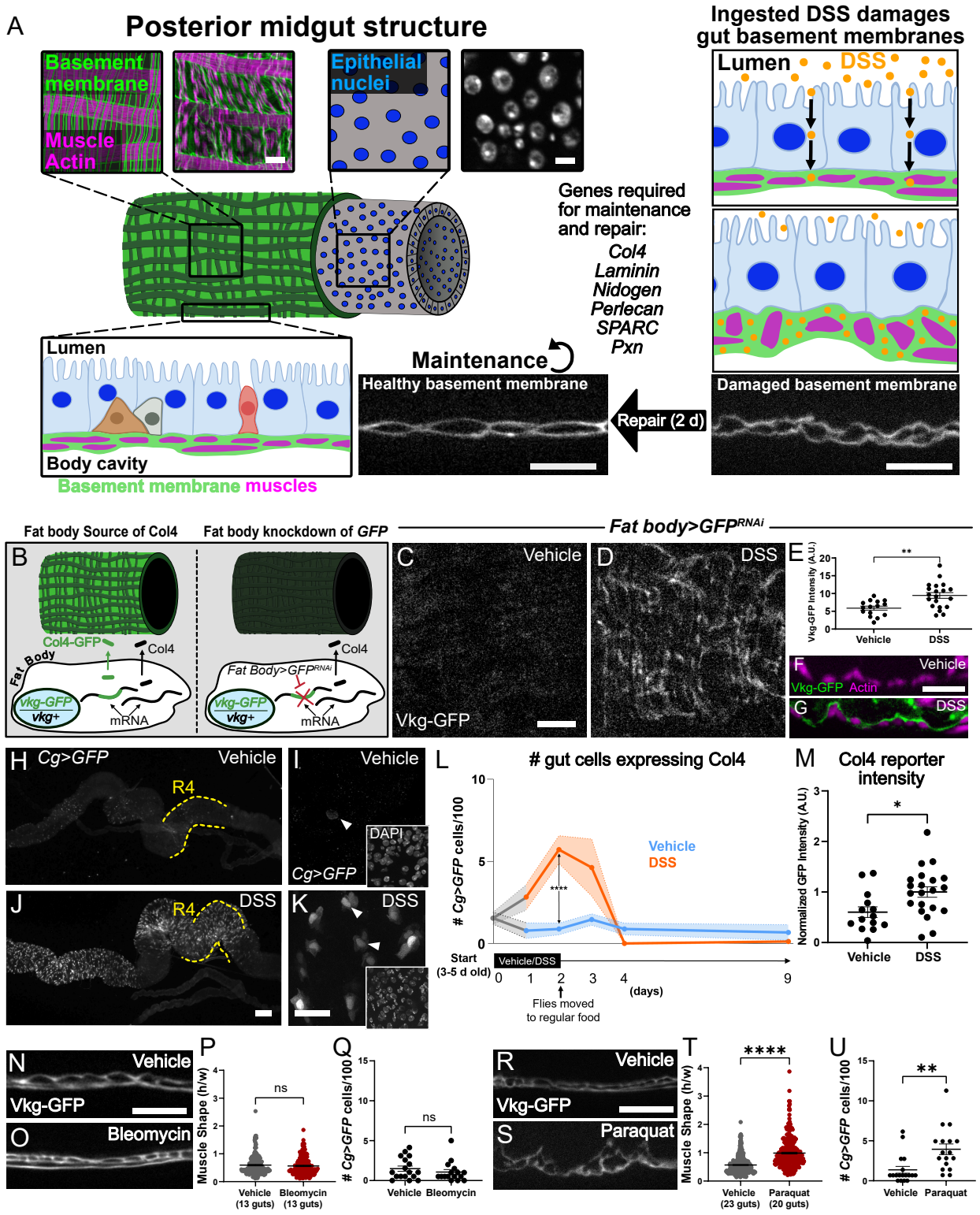
A
Posterior midgut structure
Basement membrane
Muscle Actin
Epithelial nuclei
Lumen
Body cavity
Basement membrane muscles
Genes required for maintenance and repair:
Col4
Laminin
Nidogen
Perlecan
SPARC
Pxn
Maintenance
Healthy basement membrane
Repair (2 d)
Damaged basement membrane
Ingested DSS damages gut basement membranes
Lumen
DSS
Fat body Source of Col4
Fat body knockdown of GFP
Fat body>GFP^RNAi
B
Col4-GFP
Col4
Fat Body
vkg-GFP
vkg+
mRNA
Fat Body>GFP^RNAi
C
Vehicle
Vkg-GFP
D
DSS
E
Vkg-GFP Intensity (A.U.)
Vehicle
DSS
F
Vehicle
Vkg-GFP Actin
G
DSS
H
Cg>GFP
Vehicle
R4
I
Vehicle
DAPI
Cg>GFP
J
R4
DSS
K
DSS
L
gut cells expressing Col4
Cg>GFP cells/100
Vehicle
DSS
Start (3-5 d old)
Vehicle/DSS
(days)
Flies moved to regular food
M
Col4 reporter intensity
Normalized GFP Intensity (A.U.)
Vehicle
DSS
N
Vehicle
Vkg-GFP
O
Bleomycin
P
Muscle Shape (h/w)
ns
Vehicle (13 guts)
Bleomycin (13 guts)
Q
Cg>GFP cells/100
ns
Vehicle
Bleomycin
R
Vehicle
Vkg-GFP
S
Paraquat
T
Muscle Shape (h/w)
Vehicle (23 guts)
Paraquat (20 guts)
U
Cg>GFP cells/100
Vehicle
Paraquat

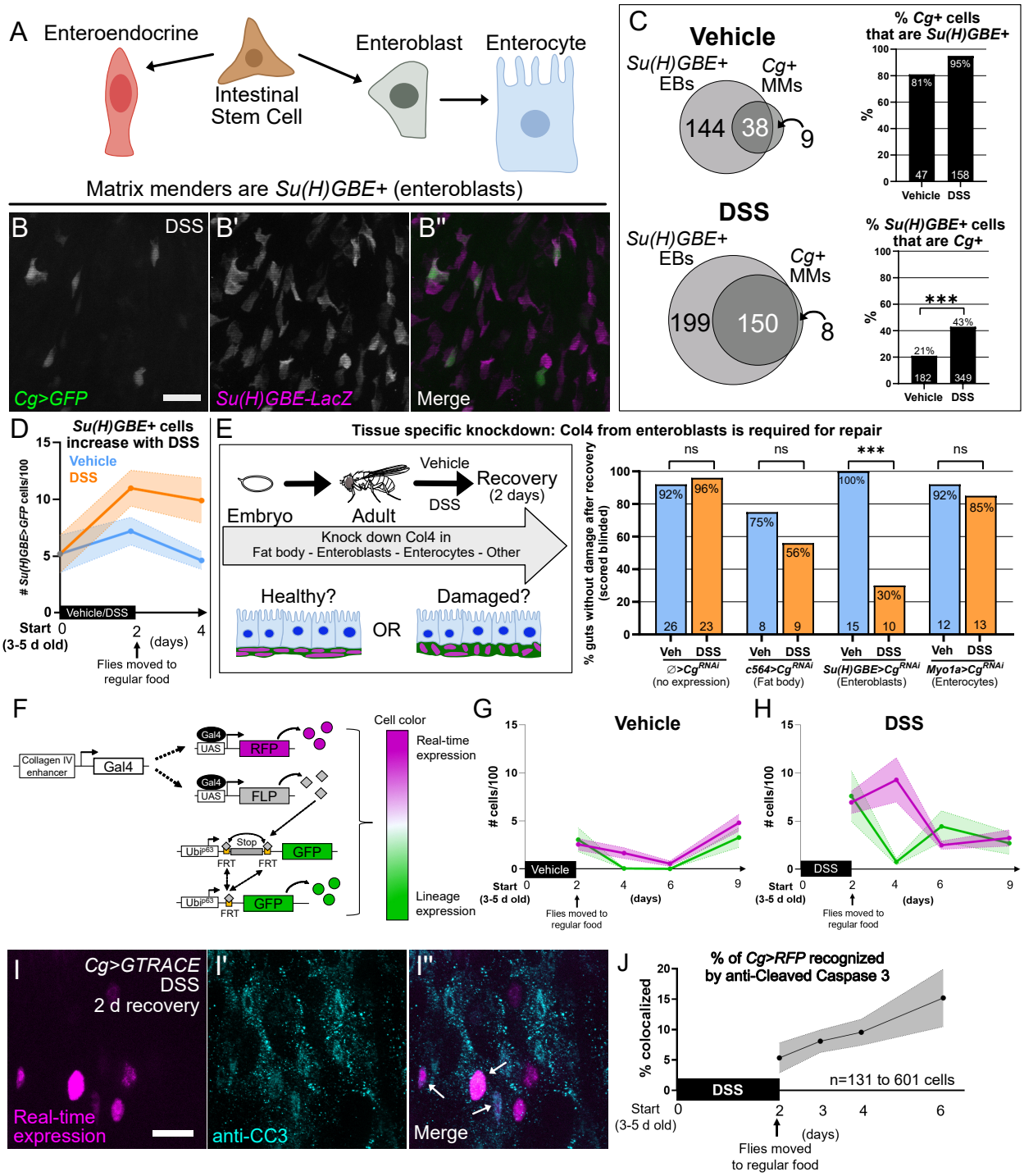
A
Enteroendocrine
Intestinal Stem Cell
Enteroblast
Enterocyte
Matrix menders are Su(H)GBE+ (enteroblasts)
B
DSS
Cg>GFP
B'
Su(H)GBE-LacZ
B''
Merge
C
Vehicle
Su(H)GBE+ EBs
Cg+ MMs
144
38
9
% Cg+ cells that are Su(H)GBE+
81%
95%
47
158
Vehicle
DSS
DSS
Su(H)GBE+ EBs
Cg+ MMs
199
150
8
% Su(H)GBE+ cells that are Cg+
***
21%
43%
182
349
Vehicle
DSS
D
Su(H)GBE+ cells increase with DSS
Vehicle
DSS
Su(H)GBE>GFP cells/100
Vehicle/DSS
Start (3-5 d old)
(days)
Flies moved to regular food
E
Tissue specific knockdown: Col4 from enteroblasts is required for repair
Embryo
Adult
Vehicle
DSS
Recovery (2 days)
Knock down Col4 in
Fat body - Enteroblasts - Enterocytes - Other
Healthy?
OR
Damaged?
% guts without damage after recovery (scored blinded)
ns
ns
***
ns
92%
96%
75%
56%
100%
30%
92%
85%
26
23
8
9
15
10
12
13
Veh
DSS
∅>Cg RNAi (no expression)
c564>Cg RNAi (Fat body)
Su(H)GBE>Cg RNAi (Enteroblasts)
Myo1a>Cg RNAi (Enterocytes)
F
Collagen IV enhancer
Gal4
UAS
RFP
FLP
Stop
GFP
FRT
Cell color
Real-time expression
Lineage expression
G
Vehicle
cells/100
Start (3-5 d old)
(days)
Flies moved to regular food
H
DSS
cells/100
Start (3-5 d old)
(days)
Flies moved to regular food
I
Cg>GTRACE
DSS
2 d recovery
Real-time expression
I'
anti-CC3
I''
Merge
J
% of Cg>RFP recognized by anti-Cleaved Caspase 3
% colocalized
DSS
n=131 to 601 cells
Start (3-5 d old)
(days)
Flies moved to regular food

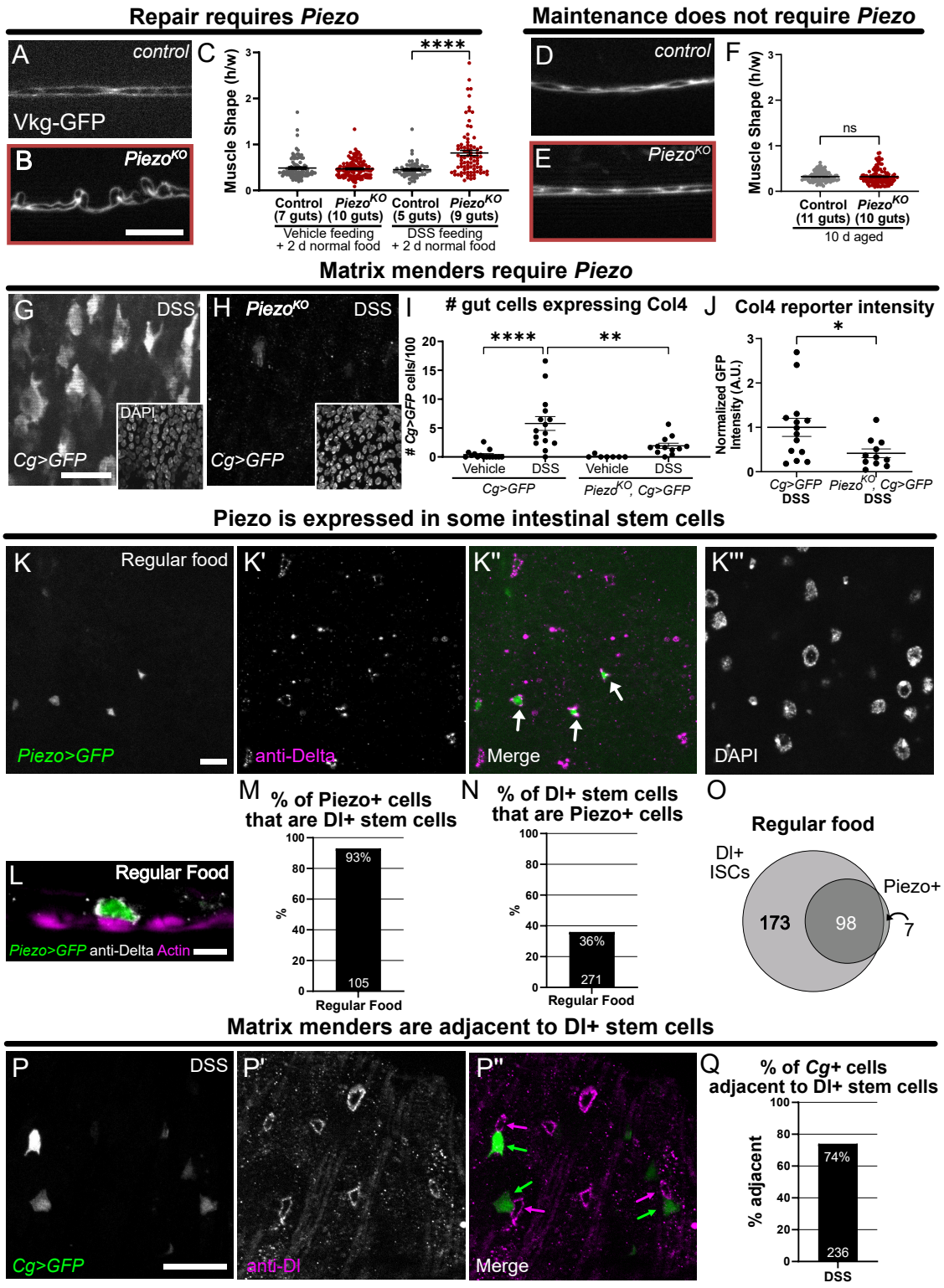
Repair requires Piezo
Maintenance does not require Piezo
A
control
Vkg-GFP
B
PiezoKO
C
Muscle Shape (h/w)
****
Control (7 guts)
PiezoKO (10 guts)
Control (5 guts)
PiezoKO (9 guts)
Vehicle feeding + 2 d normal food
DSS feeding + 2 d normal food
D
control
E
PiezoKO
F
Muscle Shape (h/w)
ns
Control (11 guts)
PiezoKO (10 guts)
10 d aged
Matrix menders require Piezo
G
DSS
DAPI
Cg>GFP
H
PiezoKO
DSS
Cg>GFP
I
gut cells expressing Col4
Cg>GFP cells/100
****
**
Vehicle
DSS
Vehicle
DSS
Cg>GFP
PiezoKO, Cg>GFP
J
Col4 reporter intensity
Normalized GFP Intensity (A.U.)
*
Cg>GFP DSS
PiezoKO, Cg>GFP DSS
Piezo is expressed in some intestinal stem cells
K
Regular food
Piezo>GFP
K'
anti-Delta
K''
Merge
K'''
DAPI
L
Regular Food
Piezo>GFP anti-Delta Actin
M
% of Piezo+ cells that are Dl+ stem cells
%
93%
105
Regular Food
N
% of Dl+ stem cells that are Piezo+ cells
%
36%
271
Regular Food
O
Regular food
Dl+ ISCs
Piezo+
173
98
7
Matrix menders are adjacent to Dl+ stem cells
P
DSS
Cg>GFP
P'
anti-Dl
P''
Merge
Q
% of Cg+ cells adjacent to Dl+ stem cells
% adjacent
74%
236
DSS

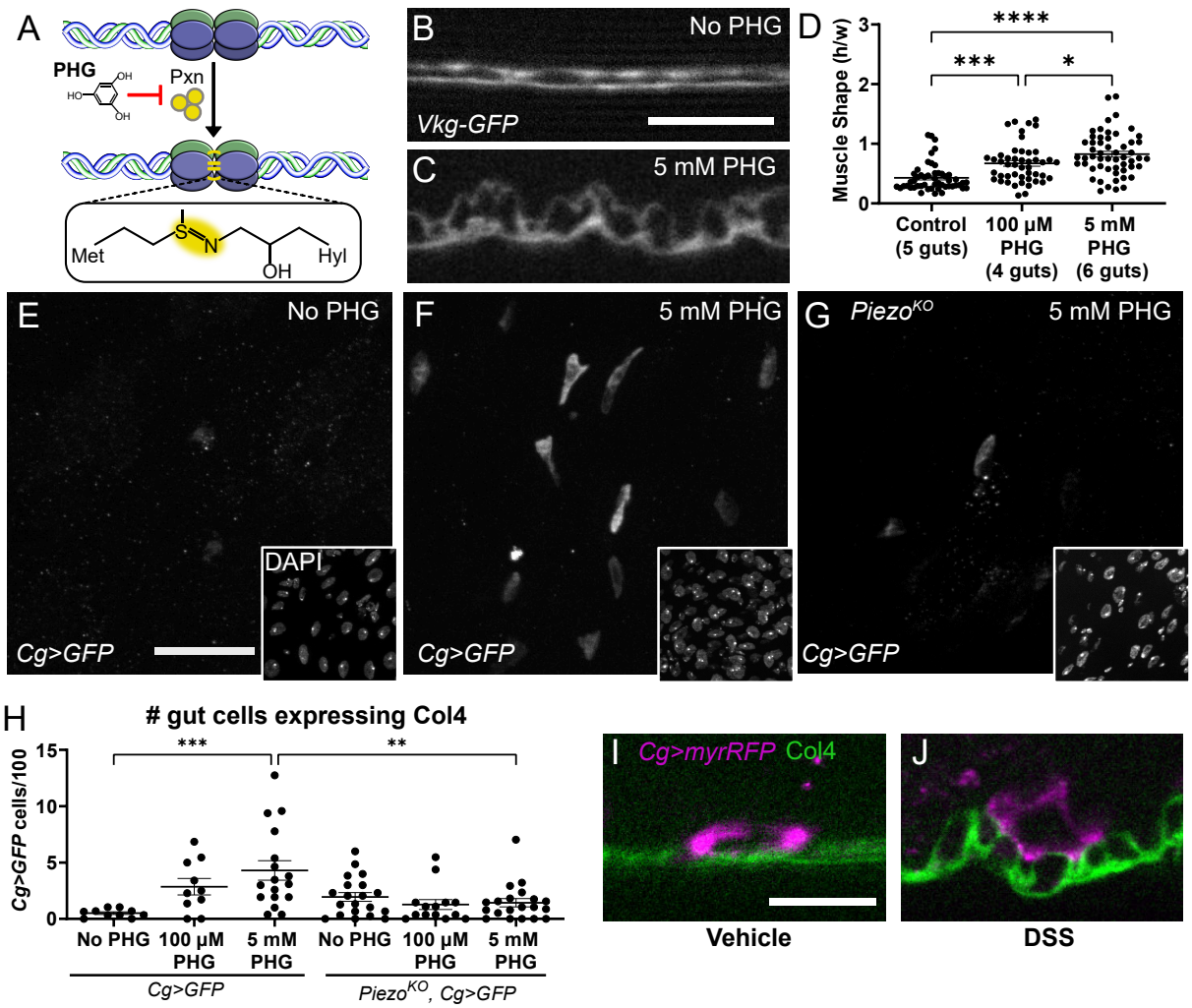
A
PHG
Pxn
Met
Hyl
OH
B
No PHG
Vkg-GFP
C
5 mM PHG
D
Muscle Shape (h/w)
****
***
*
Control (5 guts)
100 µM PHG (4 guts)
5 mM PHG (6 guts)
E
No PHG
DAPI
Cg>GFP
F
5 mM PHG
Cg>GFP
G
Piezo^KO
5 mM PHG
Cg>GFP
H
gut cells expressing Col4
Cg>GFP cells/100
***
**
No PHG
100 µM PHG
5 mM PHG
Cg>GFP
Piezo^KO, Cg>GFP
I
Cg>myrRFP Col4
Vehicle
J
DSS

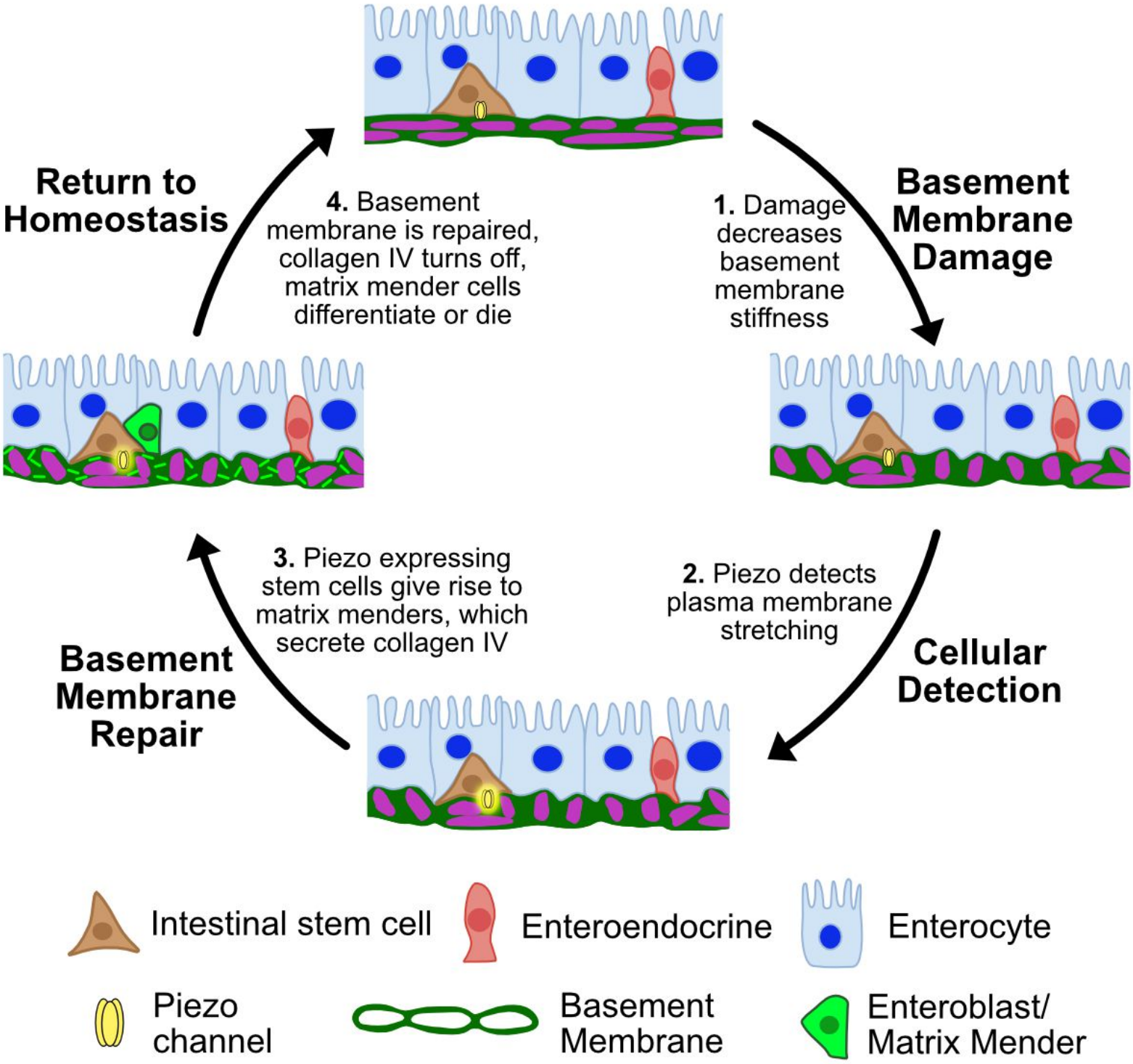
Basement Membrane Damage
1. Damage decreases basement membrane stiffness
Cellular Detection
2. Piezo detects plasma membrane stretching
Basement Membrane Repair
3. Piezo expressing stem cells give rise to matrix menders, which secrete collagen IV
Return to Homeostasis
4. Basement membrane is repaired, collagen IV turns off, matrix mender cells differentiate or die
Intestinal stem cell
Enteroendocrine
Enterocyte
Piezo channel
Basement Membrane
Enteroblast/ Matrix Mender